

A. Deltuva

# Momentum-space calculation of $^4\text{He}$ triatomic system with realistic potential

Received: date / Accepted: date

**Abstract** The system of three  $^4\text{He}$  atoms with realistic interactions is studied in the momentum-space framework. It is demonstrated that short and long-range difficulties encountered in the coordinate-space calculations can be reliably resolved in the momentum-space calculations. Well-converged and accurate results are obtained for the ground and excited trimer energies, atom-dimer scattering length, phase shifts, inelasticity parameters, and elastic and breakup cross sections. A significant correction to previously published results is found for the elastic cross section at very low energy.

**Keywords** Transition operators · three-particle scattering

**PACS** 34.50.-s · 34.10.+x

## 1 Introduction

Systems of  $^4\text{He}$  atoms have attracted significant interest, both experimentally and theoretically. The main reason is a special feature of  $^4\text{He}$  few-atom clusters, namely, an extremely weak binding of few-body ground states. This weakness of binding is responsible for the manifestation of phenomena such as the Efimov physics or superfluidity; see Ref. [1] for an overview. The understanding of these phenomena requires precise theoretical calculations of the properties of cold  $^4\text{He}$  few-body systems; up to now such calculations with realistic interaction models predominantly have been performed in various coordinate-space frameworks. Three-atom bound (trimer) and scattering states have been calculated solving Faddeev equations [1; 2; 3] or using adiabatic hyperspherical approach [4], while tetramer properties have been obtained solving the Faddeev-Yakubovsky equations [3], using the variational Gaussian expansion method [5] or the hyperspherical Monte-Carlo approach [6]. The latter was extended to more than four atoms and provided estimates for scattering lengths, whereas Ref. [3] produced results also for the atom-trimer scattering at finite energy.

The dynamics of cold  $^4\text{He}$  atoms is essentially governed by the local two-atom potential; there exist a number of realistic parametrizations [7]. Main features of those realistic potentials are long attractive van der Waals tail and a very strong repulsion at short distances. Especially the latter causes difficulties in calculations of systems containing three or more  $^4\text{He}$  atoms. Indeed, even a special form of the differential three-particle Faddeev equations with hard-core potentials has been developed and applied for the study of the three- [1] and four-atom systems [3]. Another difficulty, encountered in the scattering calculations, is a slow convergence of the results with the employed grid size [1; 2; 3]. To avoid these difficulties, simplified dynamic models based of short-range soft or separable potentials

---

A. Deltuva  
Institute of Theoretical Physics and Astronomy, Vilnius University, A. Goštauto 12, LT-01108 Vilnius, Lithuania  
E-mail: arnoldas.deltuva@tfai.vu.lt

have been invented and used in coordinate- [8] and momentum-space calculations [9]; despite their simplicity such models are quite reliable for the study of Efimov physics.

Given the success of momentum-space three-nucleon scattering calculations [10; 11], one may raise the question whether the above difficulties in the description of atomic  $^4\text{He}$  systems with realistic potentials can be resolved in the framework of momentum-space integral equations for the transition operators. Therefore the goal of the present work is to study the  $^4\text{He}$  trimer and three-atom scattering processes employing the momentum-space methods. Since the  $^4\text{He}$  triatomic system has already been investigated using several coordinate-space methods [1; 2; 3; 4; 5], in this work I will concentrate on demonstrating the reliability of momentum-space calculations with realistic potentials and providing highly accurate benchmark results. The considered observables are the trimer binding energy, atom-dimer scattering length, phase shifts, inelasticity parameters, inclusive cross sections as well as differential cross section for the atom-dimer breakup; the latter is most difficult to obtain in the coordinate-space framework and, to the best of my knowledge, has not yet been calculated.

Among the variety of realistic atomic  $^4\text{He}$  potentials, the one by Aziz and Slaman, called LM2M2 [7], is probably most widely used and therefore is an optimal choice for a benchmark calculation; having van der Waals tail and very strong short-range repulsion its behaviour is characteristic for all realistic  $^4\text{He}$  potentials. The fact that LM2M2 does not include the retardation correction which may be quite significant [4] is irrelevant for demonstrating the abilities of the method. As in most previous calculations the value of  $^4\text{He}$  mass  $m$  given by the relation  $\hbar^2/m = 12.12 \text{ K\AA}^2$  is used.

In Sec. 2 I describe the employed three-atom equations and the technical framework. In Sec. 3 I present results for the  $^4\text{He}$  trimer and atom-dimer scattering. I summarize in Sec. 4.

## 2 Integral equations for three-atom bound state and scattering

In order to apply the momentum-space techniques to the three-body problem one has to formulate it in the integral representation. In this way the asymptotic boundary conditions are implicitly built into the form of equations but lead to kernels with integrable singularities. Considering the three  $^4\text{He}$  atoms as identical bosons it is most convenient to use the symmetrized form of Faddeev equations in the Alt-Grassberger-Sandhas (AGS) version [12]; formally they coincide with the ones employed for the fermionic three-nucleon system [10; 11]. The only difference is in the properties of the basis states, namely, they must be symmetric under the exchange of particles within pair (12) which is chosen as a representative pair. The potential  $v$  acting within this pair in the integral formulation is summed up into the respective two-particle transition matrix using the Lippmann-Schwinger equation

$$t = v + vG_0t, \quad (1)$$

with  $G_0 = (E + i0 - H_0)^{-1}$  being the free Green's function of the three-particle system with energy  $E$  and kinetic energy operator  $H_0$ . The required full symmetry of the three-boson system is ensured by the operator  $P = P_{12}P_{23} + P_{13}P_{23}$  where  $P_{ab}$  is the permutation operator of particles  $a$  and  $b$ . With these definitions the Faddeev amplitude  $|\psi\rangle$  of the trimer wave function  $|B\rangle = (1 + P)|\psi\rangle$  is the solution of the homogeneous Faddeev equation

$$|\psi\rangle = G_0tP|\psi\rangle \quad (2)$$

at  $E = -E_t$  with  $E_t$  being the binding energy.

In the case of the atom-dimer scattering the AGS equations are formulated for three-particle transition operator

$$U = PG_0^{-1} + PtG_0U; \quad (3)$$

it contains the full information about the scattering process. The amplitude for the elastic scattering is obtained from the on-shell matrix element  $\langle\phi_{\mathbf{q}_f}|U|\phi_{\mathbf{q}_i}\rangle$  where  $|\phi_{\mathbf{q}_j}\rangle$  is the atom-dimer channel state given by the product of the dimer wave function  $|\phi\rangle$  and plane wave with the relative atom-dimer momentum  $\mathbf{q}_j$ . The latter is related to the available energy  $E$  as  $E = -e_d + q_j^2/2\mu$  with  $e_d$  being the dimer binding energy and  $\mu = 2m/3$  the reduced mass. The breakup amplitudes  $\langle\mathbf{p}\mathbf{q}|U_0|\phi_{\mathbf{q}_i}\rangle$ , with  $\mathbf{p}$  and  $\mathbf{q}$  being the Jacobi momenta of three free particles in the final state, are obtained as on-shell matrix elements of the breakup operator

$$U_0 = (1 + P)G_0^{-1} + (1 + P)tG_0U. \quad (4)$$

The above equations are solved in the momentum-space partial-wave basis  $|pq(Ll)JM\rangle$  where  $p$  and  $q$  are magnitudes of the Jacobi momenta and  $L$  ( $l$ ) is the orbital angular momentum for the relative motion within the pair (between the pair and spectator), coupled to the total angular momentum  $J$  with the projection  $M$ . The solution technique employs the same numerical methods as in the three-nucleon scattering calculations, i.e., real-axis integration with subtraction and special weights, spline interpolation, and Padé summation. Further details can be found in Refs. [11; 13].

However, prior to solving Eqs. (1-3) one has to transform the coordinate space potential  $V(r)$  to the momentum-space partial wave representation

$$\langle p'L|V|pL\rangle = \frac{2}{\pi} \int_0^\infty j_L(p'r)V(r)j_L(pr)r^2 dr, \quad (5)$$

where  $j_L(x)$  is the spherical Bessel function of the order  $L$ . Given the two difficulties encountered in the coordinate-space calculations, the essential questions for the momentum-space calculations are: (i) To what extent the hard core region is important and causes difficulties; (ii) At what distances the van der Waals tail becomes irrelevant. In the latter case, given the fact that the integral form of scattering equations implicitly incorporates the asymptotic boundary conditions, one may expect significant reduction in the distance  $r_{\max}$  up to which the  $r$ -space integration needs to be performed. In order to answer these questions I introduce a modified potential

$$\langle p'L|v|pL\rangle = \frac{2}{\pi} \int_0^{r_{\max}} j_L(p'r) \{ \Theta(r_{\min} - r)V(r_{\min})[2 - e^{\kappa(r_{\min} - r)}] + \Theta(r - r_{\min})V(r) \} j_L(pr)r^2 dr, \quad (6)$$

where the step function  $\Theta(x)$  equals 1 if  $x > 0$  and 0 otherwise. The parameter  $\kappa$  is chosen as  $\kappa = V'(r_{\min})/V(r_{\min})$  thereby ensuring the continuity of the derivative  $V'(r)$  and the smoothness of the modified potential at  $r = r_{\min}$ . Note that in the limit  $r_{\min} \rightarrow 0$ ,  $r_{\max} \rightarrow \infty$  one has  $\langle p'L|v|pL\rangle = \langle p'L|V|pL\rangle$ . The  $r$ -integration in Eq. (6) is performed numerically using the standard Gaussian quadrature. As the integral is one-dimensional, one may easily include several thousands or even more grid points and obtain very accurate results for  $\langle p'L|v|pL\rangle$ . These matrix elements via Eqs. (1-4) are used to calculate various three-atom observables whose dependence on the parameters  $r_{\min}$  and  $r_{\max}$  is then investigated. The findings are presented in the next section.

### 3 Results

I start by demonstrating the convergence of obtained results with  $r_{\min}$  and  $r_{\max}$ . The example observables are the dimer binding energy  $e_d$ , the trimer ground and excited state binding energies  $E_t$  and  $E_{t^*}$ , the atom-dimer scattering length  $a_0$ , and phase shifts  $\delta_l$  and inelasticity parameters  $\eta_l$  of the atom-dimer scattering at the kinetic center-of-mass (c.m.) energy  $E_k = 40$  mK. The relation between these scattering parameters and partial-wave on-shell elements  $\langle \phi q_i l | U | \phi q_i l \rangle$  of the transition operator is given by

$$a_0 = \pi\mu \langle \phi 00 | U | \phi 00 \rangle, \quad (7a)$$

$$\eta_l e^{2i\delta_l} = 1 - 2\pi i \mu q_i \langle \phi q_i l | U | \phi q_i l \rangle. \quad (7b)$$

The results are converged with respect to the number of grid points for the Jacobi momenta  $p$  and  $q$ , taking about 80 to 100 points for each momentum, and with respect to the number of partial waves, including states with  $L \leq 12$ . In the latter case the observed convergence pattern for  $E_t$ ,  $E_{t^*}$ , and  $a_0$  is in full agreement with the coordinate-space Faddeev results of Ref. [3]. To achieve the given accuracy for  $\delta_l$  and  $\eta_l$  it is sufficient to include the states with  $L \leq 10$ .

By inspecting the Table 1 one may conclude that, within the given accuracy, the results become independent of  $r_{\min}$  for  $r_{\min} \leq 1.7$  Å and independent of  $r_{\max}$  for  $r_{\max} \geq 75$  Å. For comparison, to get  $a_0$  with a comparable precision when solving coordinate-space equations, the integration up to distances well above 1000 Å was needed [1; 2; 3]. Thus, the integral formulation of the scattering problem with implicitly imposed boundary conditions allows indeed for a significant reduction in the maximal interparticle distance. The converged values agree well with the most accurate ones provided

| $r_{\min}$ | $r_{\max}$ | $e_d$  | $E_t$  | $E_{t^*}$ | $a_0$  | $\delta_0$ | $\eta_0$ | $\delta_1$ | $\eta_1$ |
|------------|------------|--------|--------|-----------|--------|------------|----------|------------|----------|
| 1.5        | 25         | 1.3010 | 126.40 | 2.267     | 115.32 | 24.92      | 0.8281   | -73.78     | 0.7671   |
| 1.5        | 50         | 1.3034 | 126.40 | 2.271     | 115.22 | 24.93      | 0.8283   | -73.78     | 0.7675   |
| 1.5        | 75         | 1.3035 | 126.40 | 2.271     | 115.21 | 24.93      | 0.8283   | -73.78     | 0.7676   |
| 1.5        | 100        | 1.3035 | 126.40 | 2.271     | 115.21 | 24.93      | 0.8283   | -73.78     | 0.7676   |
| 1.5        | 200        | 1.3035 | 126.40 | 2.271     | 115.21 | 24.93      | 0.8283   | -73.78     | 0.7676   |
| 0.0        | 100        | 1.3035 | 126.40 | 2.271     | 115.21 | 24.93      | 0.8283   | -73.78     | 0.7676   |
| 0.5        | 100        | 1.3035 | 126.40 | 2.271     | 115.21 | 24.93      | 0.8283   | -73.78     | 0.7676   |
| 1.0        | 100        | 1.3035 | 126.40 | 2.271     | 115.21 | 24.93      | 0.8283   | -73.78     | 0.7676   |
| 1.5        | 100        | 1.3035 | 126.40 | 2.271     | 115.21 | 24.93      | 0.8283   | -73.78     | 0.7676   |
| 1.7        | 100        | 1.3035 | 126.40 | 2.271     | 115.21 | 24.93      | 0.8283   | -73.78     | 0.7676   |
| 1.8        | 100        | 1.3041 | 126.41 | 2.272     | 115.22 | 24.93      | 0.8283   | -73.78     | 0.7677   |
| 1.9        | 100        | 1.3093 | 126.51 | 2.278     | 115.36 | 24.93      | 0.8284   | -73.76     | 0.7687   |
| 2.0        | 100        | 1.3434 | 127.13 | 2.321     | 116.23 | 24.95      | 0.8290   | -73.64     | 0.7754   |

**Table 1** Observables in three-atom system as functions of the coordinate-space cut-off parameters  $r_{\min}$  and  $r_{\max}$  that are given in units of  $\text{\AA}$ . Dimer binding energy  $e_d$ , trimer binding energy for ground and excited state  $E_t$  and  $E_{t^*}$  (all in units of mK), atom-dimer scattering length  $a_0$  (in units of  $\text{\AA}$ ), and phase shifts  $\delta_l$  (in degrees) and inelasticity parameters  $\eta_l$  for the atom-dimer scattering at  $E_k = 40$  mK are listed.

in the literature [3; 5; 14] for  $E_t$ ,  $E_{t^*}$ , and  $a_0$ ; this comparison is presented in Table 2. The expectation values for internal kinetic energies of trimer states  $\langle K_t \rangle$  and  $\langle K_{t^*} \rangle$  show good agreement as well. The hyperspherical Monte-Carlo approach [6] is less accurate for  $a_0$ , while the differences between the results of [1] and [3; 5; 14] are due to the limitation  $L \leq 4$  used in Ref. [1].

| Reference | $E_t$   | $\langle K_t \rangle$ | $E_{t^*}$ | $\langle K_{t^*} \rangle$ | $a_0$  |
|-----------|---------|-----------------------|-----------|---------------------------|--------|
| This work | 126.40  | 1660.5                | 2.271     | 122.13                    | 115.21 |
| [3]       | 126.39  | 1658                  | 2.268     | 122.1                     | 115.2  |
| [5]       | 126.40  | 1660.4                | 2.2706    | 122.15                    |        |
| [2; 15]   | 126.41  |                       | 2.271     |                           | 115.4  |
| [14]      | 126.394 |                       | 2.2711    |                           | 115.22 |
| [1]       | 125.9   |                       | 2.28      |                           | 117.0  |
| [6]       | 125.5   |                       | 2.19      |                           | 126    |

**Table 2** Trimer properties and atom-dimer scattering length as obtained in different works.  $a_0$  is given in units of  $\text{\AA}$  while other quantities in units of mK.

Regarding the atom-dimer scattering at finite energies, the available results are scarce and lack consistency. For example, the  $S$ -wave ( $l = 0$ ) phase shifts  $\delta_0$  show some disagreements between Refs. [1; 2; 4].  $\delta_0$  values below breakup threshold are tabulated in Ref. [2], however, it appears that Ref. [2] uses a nonstandard convention which makes the comparison ambiguous. Indeed, while the standard relation between  $a_0$  and  $\delta_0$  reads  $\lim_{q_i \rightarrow 0} \tan \delta_0/q_i = -a_0$ , an inspection of  $\delta_0$  results from Ref. [2] reveals the relation  $\lim_{q_i \rightarrow 0} \sqrt{4/3} \tan \delta_0/q_i = -a_0$ . This may also explain why  $\delta_0$  values from Ref. [2] are higher than those of Ref. [1]. To sort these discrepancies I present in Table 3 highly accurate momentum-space results for atom-dimer phase shifts  $\delta_l$  and inelasticity parameters  $\eta_l$  up to  $l = 5$ . A broad range of kinetic energies in the c.m. system is considered, ranging from 0.1 mK to 40 mK which is well above the breakup threshold of 1.3035 mK.

In addition, elastic cross section and breakup rate results, albeit with a different potential, are given in Ref. [4]. However, the elastic cross section  $\sigma_e$  in Ref. [4] shows a very strange energy dependence in partial waves with  $l > 0$ : at  $E_k = 0.001$  mK the partial cross sections  $\sigma_e(l)$  are large but decrease with increasing energy in contrast to the standard near-threshold behaviour, and, furthermore,  $\sigma_e(l)$  show the trend to increase with increasing  $l$  such that one can even question the partial-wave convergence. Such a strange behaviour is absent in the momentum-space results displayed in Fig. 1. Below 0.1 mK the elastic cross section is almost constant and strongly dominated by the  $l = 0$  state, whereas very small  $l > 0$  contributions increase with increasing energy and decrease with increasing  $l$ . This is not unexpected given the energy evolution of phase shifts  $\delta_l$  in Table 3 that show a similar trend. One might suspect that larger distances in Eq. (6) become more important at very low energies. To verify the convergence of the results I performed additional calculations with  $r_{\max}$  up to 4000  $\text{\AA}$ , but found no changes to the results of Fig. 1. Note, however, that due to the van der Waals tail  $1/r^6$  the phase

| $E_k$ | $\delta_0$ | $\eta_0$ | $\delta_1$ | $\eta_1$ | $\delta_2$ | $\eta_2$ | $\delta_3$ | $\eta_3$ | $\delta_4$ | $\eta_4$ | $\delta_5$ | $\eta_5$ |
|-------|------------|----------|------------|----------|------------|----------|------------|----------|------------|----------|------------|----------|
| 0.1   | 158.05     | 1.0000   | -2.39      | 1.0000   | 0.11       | 1.0000   | -0.00      | 1.0000   | 0.00       | 1.0000   | -0.00      | 1.0000   |
| 0.2   | 149.11     | 1.0000   | -5.40      | 1.0000   | 0.44       | 1.0000   | -0.03      | 1.0000   | 0.00       | 1.0000   | -0.00      | 1.0000   |
| 0.4   | 137.11     | 1.0000   | -10.76     | 1.0000   | 1.51       | 1.0000   | -0.17      | 1.0000   | 0.02       | 1.0000   | -0.00      | 1.0000   |
| 1.0   | 116.71     | 1.0000   | -21.81     | 1.0000   | 4.91       | 1.0000   | -0.96      | 1.0000   | 0.20       | 1.0000   | -0.04      | 1.0000   |
| 2.0   | 99.04      | 0.9994   | -32.32     | 1.0000   | 8.12       | 0.9995   | -2.23      | 1.0000   | 0.62       | 1.0000   | -0.18      | 1.0000   |
| 4.0   | 80.79      | 0.9989   | -43.48     | 0.9996   | 10.33      | 0.9833   | -3.60      | 0.9981   | 1.17       | 0.9997   | -0.42      | 1.0000   |
| 10.0  | 57.52      | 0.9853   | -57.30     | 0.9840   | 11.27      | 0.8878   | -4.50      | 0.9775   | 1.54       | 0.9943   | -0.67      | 0.9987   |
| 20.0  | 40.90      | 0.9319   | -66.05     | 0.9187   | 11.41      | 0.7696   | -4.30      | 0.9364   | 1.43       | 0.9795   | -0.70      | 0.9935   |
| 40.0  | 24.93      | 0.8283   | -73.78     | 0.7676   | 11.84      | 0.6610   | -3.43      | 0.8782   | 1.26       | 0.9527   | -0.59      | 0.9807   |

**Table 3** Atom-dimer phase shifts  $\delta_l$  (in degrees) and inelasticity parameters  $\eta_l$  as functions of the kinetic energy  $E_k$  (in mK) in the c.m. system.

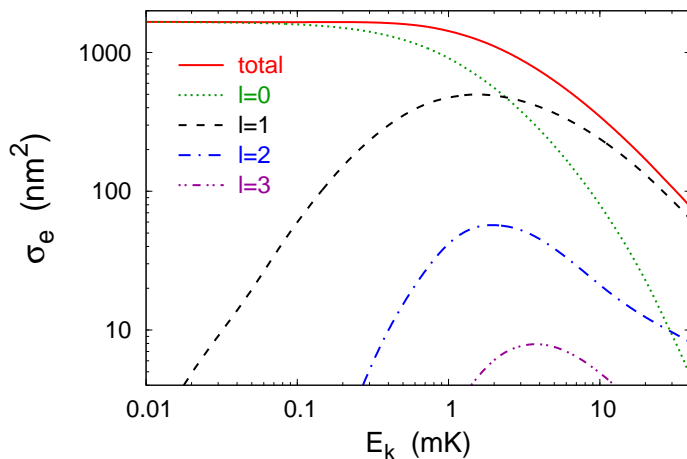


**Fig. 1** (Color online) Atom-dimer total elastic cross section and its partial-wave contributions as functions the c.m. kinetic energy. Contributions with  $l \geq 4$  remain well below  $2 \text{ nm}^2$ .

shifts  $\delta_l$  and partial cross sections  $\sigma_e(l)$  follow the standard near-threshold behaviour  $\delta_l \sim q_i^{2l+1}$  and  $\sigma_e(l) \sim E_k^{2l}$  only for low  $l$ .

Regarding the total breakup cross section  $\sigma_b$ , there is a good qualitative agreement between the present momentum-space results displayed in Fig. 2 and those of Ref. [4] extracted from the breakup rate  $\sigma_b q_i / \mu$ . Above  $E_k = 3 \text{ mK}$  in both cases  $\sigma_b$  is dominated by initial states  $l = 2$  and  $3$  whereas  $l = 0$  contribution is lower by an order of magnitude. Furthermore, the latter exhibits a local minimum around  $E_k = 4 \text{ mK}$  seen in Fig. 2 as well as in Ref. [4].

The rate for the time reversed reaction, the three-atom recombination, is simply proportional to  $\sigma_b$  with a kinematic factor [16] and therefore is not shown separately. These observables, owing to their inclusive character, can be obtained even without explicit calculation of breakup or recombination operator  $U_0$  but just using the optical theorem for  $U$ . Exclusive or semi-inclusive observables are more difficult to calculate, and the transition operator momentum-space framework may be the most appropriate method for such calculations, much like in the three-nucleon physics [10; 13; 17]. To demonstrate its abilities I present in Fig. 3 the angular distribution of the semi-inclusive differential cross section  $d\sigma_b/d\Omega$  and in Fig. 4 the fully exclusive fivefold differential cross section  $d^5\sigma_b/d\Omega_1 d\Omega_2 dS$ , where  $\Omega_j$  is the solid angle of the  $j$ -th atom, given by polar and azimuthal angles  $(\Theta_j, \varphi_j)$ , and  $S$  is the distance along the kinematical curve, routinely employed in three-nucleon physics [10; 13]. The energy  $E_k = 5 \text{ mK}$  is chosen such that the ratio  $E_k/e_d$  is nearly the same as for the nucleon lab energy of  $13 \text{ MeV}$  in the nucleon-deuteron breakup where numerous calculations exist [10; 13; 17].

Since higher three-body partial waves contribute to breakup and the final phase space is of higher dimension, the breakup differential cross section  $d\sigma_b/d\Omega$  exhibits a more complicated angular dependence in the breakup as compared to the elastic one  $d\sigma_e/d\Omega$  that is also shown in Fig. 3

The fully exclusive fivefold differential cross section  $d^5\sigma_b/d\Omega_1 d\Omega_2 dS$  is shown in Fig. 4 for three special kinematical configurations  $(\Theta_1, \Theta_2, \varphi_2 - \varphi_1) = (50.6^\circ, 50.6^\circ, 120.0^\circ)$ ,  $(38.9^\circ, 38.9^\circ, 180.0^\circ)$ , and

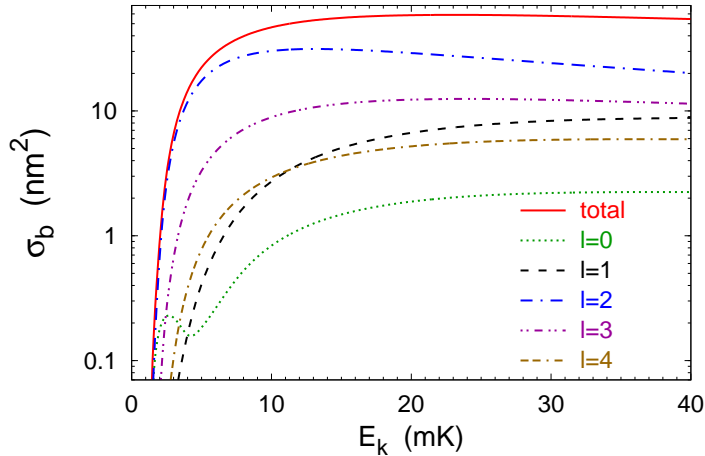


**Fig. 2** (Color online) Atom-dimer total breakup cross section and its most sizable partial-wave contributions as functions the c.m. kinetic energy.

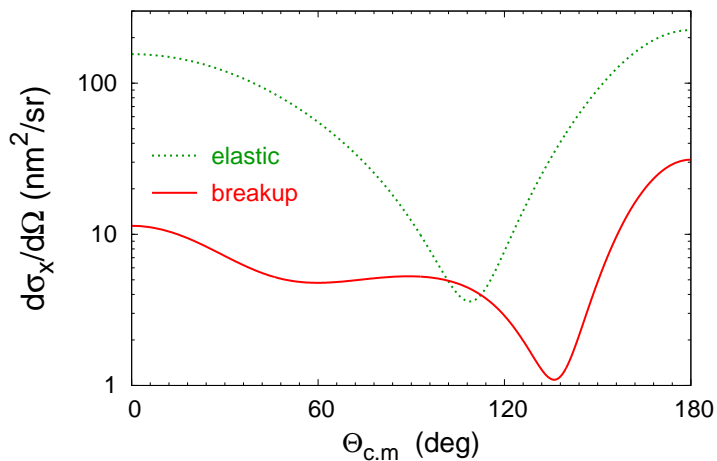


**Fig. 3** (Color online) Differential cross sections for the atom-dimer elastic scattering (dotted curve) and breakup (solid curve) at  $E_k = 5$  mK as functions of the atom scattering angle in the c.m. frame.

( $56.1^\circ, 56.1^\circ, 180.0^\circ$ ), that are called the space star, quasi free scattering (QFS), and collinear configuration, respectively [10; 17]. It is quite interesting to compare these results with the ones for the nucleon-deuteron breakup at 13 MeV in the corresponding configurations as given in Ref. [17]. Although there are some similarities, e.g., the existence of the QFS peak and of the local minimum at the collinear point (around  $S = 5$  mK in both cases), there are also significant differences, namely, (i) the reduction (for QFS and collinear) or absence (for space star) of other peaks with large cross section, and (ii) the presence of local minima with very small  $d^5\sigma_b/d\Omega_1 d\Omega_2 dS$  for  $S < 2.5$  mK and  $S_{\max} - S < 2.5$  mK. Possible explanations for these differences are following: In the case (i) the two-nucleon  $^1S_0$  virtual state is responsible, at least partially, for the differential cross section peaks observed in the nucleon-deuteron breakup; there is no similar state in the  $^4\text{He}$  atomic system. In the case (ii) the  $d^5\sigma_b/d\Omega_1 d\Omega_2 dS$  may get modulated by the nodes in the momentum-space representation of the  $^4\text{He}$  dimer wave function that are more numerous than for the deuteron.

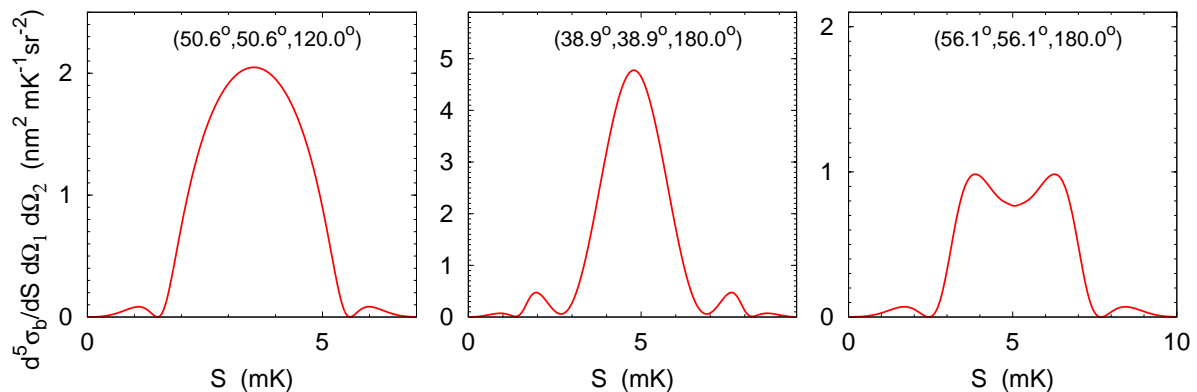


**Fig. 4** (Color online) Differential cross sections for the atom-dimer breakup at  $E_k = 5$  mK as functions of the energy parameter  $S$  in the space star (left), quasi free scattering (middle), and collinear (right) kinematical configurations.

#### 4 Summary

I performed bound state and scattering calculations in the system of three  $^4\text{He}$  atoms using realistic two-atom potential. Exact integral equations for the Faddeev amplitude and transition operators were solved in the momentum-space partial-wave framework. I demonstrated that two technical complications present in the coordinate-space calculations, i.e., the hard core and the need for a very extended grid, create no major difficulties in the momentum-space calculations, and well-converged results are obtained. Predictions for the ground and excited trimer energies and the atom-dimer scattering length agree well with the most accurate coordinate-space results obtained by other authors. I also presented high-precision benchmark results for the atom-dimer phase shifts, inelasticity parameters, and elastic and breakup cross sections over a broad energy range. An important finding in the case of low-energy elastic scattering is that the unusual energy and angular momentum dependence of partial cross sections  $\sigma_e(l)$  predicted in Ref. [4] is not confirmed; instead, a strong dominance of the  $l = 0$  wave is found in the present work while  $l \geq 1$  contributions become practically negligible for energies below 0.1 mK. Despite this disagreement, the results for the total breakup cross section in both calculations are consistent. The semi-inclusive and fully exclusive breakup differential cross sections are calculated for the first time and compared with those in the nucleon-deuteron breakup. It is conjectured that  $^4\text{He}$  dimer wave function nodes may be related to the minima of the fivefold differential cross section.

#### References

1. Kolganova, E., Motovilov, A., Sandhas, W.: Ultracold collisions in the system of three helium atoms. *Physics of Particles and Nuclei* **40**, 206 (2009).
2. Roudnev, V.: Ultra-low energy elastic scattering in a system of three He atoms. *Chem. Phys. Lett.* **367**, 95 (2003).
3. Lazauskas, R., Carbonell, J.: Description of  $\text{He}_4$  tetramer bound and scattering states. *Phys. Rev. A* **73**, 062717 (2006).
4. Suno, H., Esry, B. D.: Adiabatic hyperspherical study of triatomic helium systems. *Phys. Rev. A* **78**, 062701 (2008).
5. Hiyama, E., Kamimura, M.: Variational calculation of  $^4\text{He}$  tetramer ground and excited states using a realistic pair potential. *Phys. Rev. A* **85**, 022502 (2012).
6. Blume, D., Greene, C. H.: Monte Carlo hyperspherical description of helium cluster excited states. *J. Chem. Phys.* **112**, 8053 (2000).
7. Aziz, R. A., Slaman, M. J.: An examination of abinitio results for the helium potential energy curve. *The Journal of Chemical Physics* **94**, 8047 (1991).
8. Kievsky, A., Garrido, E., Romero-Redondo, C., Barletta, P.: The Helium Trimer with Soft-Core Potentials. *Few-Body Systems* **51**, 259 (2011).
9. Shepard, J. R.: Calculations of recombination rates for cold  $^4\text{He}$  atoms from atom-dimer phase shifts and determination of universal scaling functions. *Phys. Rev. A* **75**, 062713 (2007).
10. Glöckle, W., Witała, H., Hüber, D., Kamada, H., Golak, J.: The Three-Nucleon Continuum: Achievements, Challenges and Applications. *Phys. Rep.* **274**, 107 (1996).

- 
11. Deltuva, A., Chmielewski, K., Sauer, P. U.: Nucleon-deuteron scattering with  $\Delta$ -isobar excitation: Chebyshev expansion of two-baryon transition matrix. *Phys. Rev. C* **67**, 034001 (2003).
  12. Alt, E. O., Grassberger, P., Sandhas, W.: Reduction of the three-particle collision problem to multi-channel two-particle Lippmann-Schwinger equations. *Nucl. Phys.* **B2**, 167 (1967).
  13. Chmielewski, K., Deltuva, A., Fonseca, A. C., Nemoto, S., Sauer, P. U.: Breakup in nucleon-deuteron scattering with  $\Delta$ -isobar excitation. *Phys. Rev. C* **67**, 014002 (2003).
  14. Roudnev, V.: Ultra-low energy elastic scattering in a system of three He atoms. *Chem. Phys. Lett.* **367**, 95 (2003).
  15. Roudnev, V. A., Yakovlev, S. L., Sofianos, S. A.: Bound-State Calculations for Three Atoms Without Explicit Partial Wave Decomposition. *Few-Body Systems* **37**, 179 (2005).
  16. Deltuva, A., Fonseca, A. C.:  $^3\text{H}$  production via neutron-neutron-deuteron recombination. *Phys. Rev. C* **87**, 014002 (2013).
  17. Deltuva, A., Fonseca, A. C., Sauer, P. U.: Momentum-space description of three-nucleon breakup reactions including the Coulomb interaction. *Phys. Rev. C* **72**, 054004 (2005).